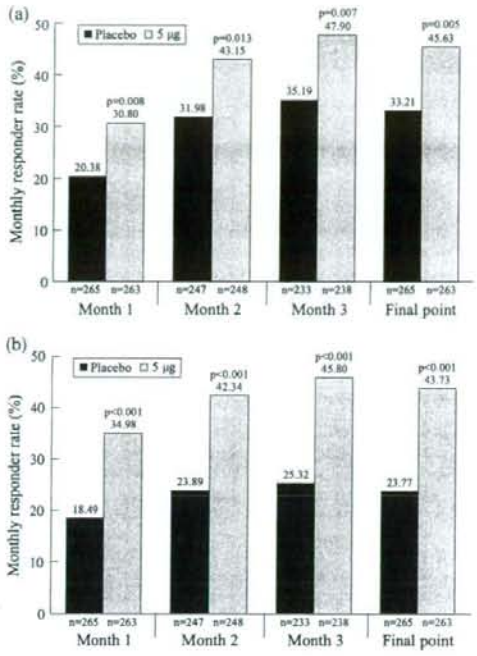

Figure 5. (a) Monthly responder rate of "Patient-reported assessment of relief of abdominal discomfort and/or pain". (b) Monthly responder rate of "Patient-reported assessment of improvement of abnormal bowel habits". *P*-values were calculated using the χ^2 test.

compared with placebos was observed at all time-points in male patients. In females, however, it was only observed at month 2. These findings may be related to the small sizes of female samples in this clinical study and a high level of placebo effect in females compared to males. The time-dependent increase in the placebo effect in females was greater than that in males. Chang & Heitkemper suggested that possible factors affecting gender differences in the response to treatment of patients with IBS included biobehavioral responses to stress, and sexual cycle, as well as differences in the roles and emotions between men and women. All of these factors may result in a variety of differences in clinical and physiological reactions [22]. Increased gastrointestinal symptoms and sensitivity of the colon during menses have been reported in clinical studies [23,24]. The mean age of female patients was around 40 years in this study, and the sexual cycle may have affected the efficacy assessment to some extent. A recent positron emission tomography study in patients with IBS reported gender differences in activation of brain networks concerned with cognitive, automatic and antinociceptive responses to

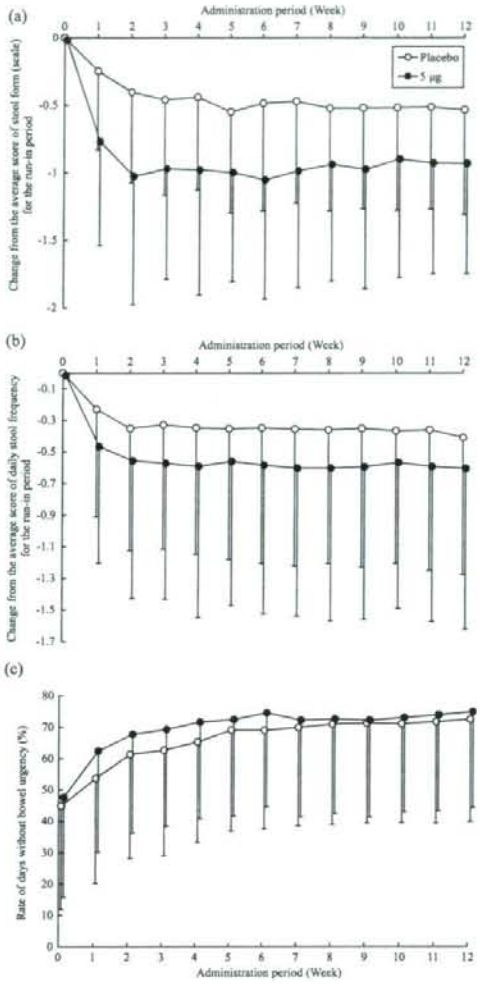

Figure 6. (a) Change in weekly average scores of stool form (change from the average score for the run-in period). (b) Change in weekly average of daily stool frequency (change from the average score for the run-in period). (c) Rate of days without bowel urgency (number of days without bowel urgency in each observation week/total number of entry days in the week).

aversive visceral stimuli or the psychological stress due to such visceral stimuli [25]. Likewise, there are physiological differences between male and female patients with IBS, but how these factors affect the response to placebos in each gender has not been elucidated. It is unclear how the differences in demographic characteristics between male and female patients affect the female patients' responses.

A clinical study of alosetron demonstrated efficacy in female patients but not in male patients [10]. The

Table II. Incidence of adverse events (incidence of 2% or higher in ramosetron group).

Symptom	Placebo	5 μg	*p*-value (χ^2 test, with continuity correction)
No. of safety analysis population	269	270	
All adverse events	141 (52.42%)	163 (60.37%)	0.076
Gastrointestinal disorders	33 (12.27%)	70 (25.93%)	<0.001
Abdominal distension	4 (1.49%)	12 (4.44%)	0.077
Abdominal pain upper	5 (1.86%)	7 (2.59%)	0.775
Constipation	5 (1.86%)	14 (5.19%)	0.063
Hard stool	2 (0.74%)	20 (7.41%)	<0.001
Immune system disorders	4 (1.49%)	6 (2.22%)	0.754
Seasonal allergy	4 (1.49%)	6 (2.22%)	0.754
Infections and infestations	72 (26.77%)	53 (19.63%)	0.063
Nasopharyngitis	54 (20.07%)	40 (14.81%)	0.135
Investigations	37 (13.75%)	43 (15.93%)	0.557
Alanine aminotransferase increased	8 (2.97%)	7 (2.59%)	0.994
Blood bilirubin increased	3 (1.12%)	6 (2.22%)	0.505
Gamma-glutamyltransferase increased	10 (3.72%)	9 (3.33%)	0.993
White blood cell count increased	7 (2.60%)	13 (4.81%)	0.258
Respiratory, thoracic and mediastinal disorders	12 (4.46%)	16 (5.93%)	0.567
Upper respiratory tract inflammation	6 (2.23%)	10 (3.70%)	0.451

No. of subjects with events (incidence).

difference in the site of action between alosetron and ramosetron is a possible cause of the gender differences in the response to these drugs. Ramosetron acts only on peripheral tissues, whereas alosetron is reportedly transferred to the brain [26]. There are gender differences in the central pathophysiology of IBS [25,27]. In response to aversive visceral stimulation, women with IBS showed greater activation in the "limbic" area, which is frequently activated by emotional stimuli including the amygdala, as well as anterior and infragenual cingulate cortices. With regard to its central effects, alosetron was found to have an inhibitory effect on "limbic" (i.e. amygdala and ventral striatum) regions, and the inhibition of amygdala activity correlated with IBS symptom improvement. It is therefore conceivable that the greater efficacy of alosetron in women with IBS may be due to its inhibitory effects in the "limbic" region of the brain, which is more abnormally activated in women than men [28], whereas ramosetron does not act on the central nervous system. This difference in the site of action between alosetron and ramosetron may contribute to the result that ramosetron was effective in both male and female patients.

Alterations in mobility, secretion and visceral sensation are hallmarks of IBS. As all of these aspects of gastrointestinal function involve serotonin signaling, potential alterations in mucosal serotonin signaling have been explored as a possible mechanism of altered function and sensation in IBS [29,30]. A significant association was observed between D-IBS female patients and the serotonin reuptake transporter protein (SERT) polymorphisms, suggesting that the serotonin transporter is a potential candidate gene for D-IBS women [31,32]. However, it is not known whether differences in SERT polymorphisms between women and men with IBS contribute to the observed differences in clinical response to 5-HT_3 receptors antagonists.

Eighty percent of the patients enrolled in this trial were male. Kumano et al. reported that D-IBS is found more frequently among males than females, i.e. 67.5% of those with D-IBS are males; conversely, C-IBS is found much more frequently among females than males, i.e. 89.9% of those with C-IBS are females, in Japan [2]. It was reported that, in the United States, C-IBS is also found more among females, but the proportion of males with D-IBS is almost the same as that of females with D-IBS [33]. It is assumed that the difference in the ratio of males to females enrolled in the trial might be related to the differences in culture or lifestyle.

Adverse events that frequently occurred during the treatment with ramosetron were abdominal distension, constipation and hard stool, which are considered to be a classic effect of the 5-HT_3 receptor antagonist. The incidence of constipation due to the administration of alosetron was 29% ($n=8328$) [34], whereas such incidence due to the administration of ramosetron was only 5.19%. Thus, the incidence of constipation in the ramosetron group was lower than that in the alosetron group. Neither ischemic colitis nor severe constipation, which were reported with alosetron use, was observed in treatment with ramosetron. Although the pathogenesis of ischemic colitis in patients with IBS on treatment

with alosetron is uncertain, ischemic colitis might result from the constipation due to slow transit induced by alosetron [35]. The incidence of constipation in the ramosetron group is considered to be lower than that in the alosetron group, so ischemic colitis is unlikely to be caused by ramosetron.

In summary, it was shown that ramosetron is also significantly effective for male patients with D-IBS, unlike alosetron. It was also shown that ramosetron seems to be effective for female patients with D-IBS. Ramosetron was also proven to be a safe drug. Ramosetron is recommended as a novel drug for the treatment of Japanese patients with D-IBS due to its selective antagonistic action on 5-HT_3 receptors.

Acknowledgements

We thank the following investigators (in alphabetical order) who participated in the study: H. Ankou; T. Arai; K. Egawa; N. Fujino; Y. Hamahata; S. Hayashi; K. Hirakawa: T. Hirose; S. Hotta; T. Ichimori; T. Inomoto; T. Ishihara; H. Ishii; T. Ishii; T. Isono; K. Ito; E. Iwashita; T. Kamoshida; H. Kaneko; S. Kawai; K. Kawakami; T. Kawano; T. Komazaki; Y. Kumagai; H. Maekawa; K. Morita; M. Murakami; H. Murata; H. Nagata; A. Nakajima; M. Nakashima; N. Nomura; H. Oizumi; S. Okamura; S. Orii; H. Sakaida; K. Sasaki; C. Sekine; E. Sekizuka; W. Shinmura; C. Sugano; H. Suzuki; T. Suzuki; Y. Suzuki; M. Takada; K. Takahashi; Y. Tei; T. Terada; S. Tokitou; M. Tomiyama; A. Torii; J. Unno; W. Yamamuro; K. Yamashita

Declaration of interest: This study was supported by Astellas Pharma Inc., Tokyo, Japan.

References

[1] Talley NJ. Irritable bowel syndrome: definition, diagnosis and epidemiology. Baillieres Best Pract Res Clin Gastroenterol 1999;13:371–84.

[2] Kumano H, Kaiya H, Yoshiuchi K, Yamanaka G, Sasaki T, Kuboki T. Comorbidity of irritable bowel syndrome, panic disorder, and agoraphobia in a Japanese representative sample. Am J Gastroenterology 2004;99:370–6.

[3] Gralnek IM, Hays RD, Kilbourne A, Naliboff B, Mayer EA. The impact of irritable bowel syndrome on health-related quality of life. Gastroenterology 2000;119:654–60.

[4] Camilleri M, Heading RC, Thompson WG. Consensus reports: clinical perspectives, mechanisms, diagnosis and management of irritable bowel syndrome. Aliment Pharmacol Ther 2002;16:1407–30.

[5] Fukudo S, Nomura T, Hongo M. Impact of corticotropin-releasing hormone on gastrointestinal motility and adrenocorticotropic hormone in normal controls and patients with irritable bowel syndrome. Gut 1998;42(6):845–9.

[6] Bouin M, Plourde V, Boivin M, Riberdy M, Lupien F, Laganiere M, et al. Rectal distention testing in patients with irritable bowel syndrome: sensitivity, specificity, and predictive values of pain sensory thresholds. Gastroenterology 2002;122:1771–7.

[7] Gershon MD. Review article: roles played by 5-hydroxytryptamine in the physiology of the bowel. Aliment Pharmacol Ther 1999;13 Suppl 2:15–30.

[8] Humphrey PPA, Bountra C, Clayton N, Kozlowski K. Review article: the therapeutic potential of 5-HT_3 receptor antagonists in the treatment of irritable bowel syndrome. Aliment Pharmacol Ther 1999;13 Suppl 2:31–8.

[9] Olden KW. Irritable bowel syndrome: An overview of diagnosis and pharmacologic treatment. Cleve Clin J Med 2003;70 Suppl 2:S3–7.

[10] Camilleri M, Mayer EA, Drossman DA, Heath A, Dukes GE, McSorley D, et al. Improvement in pain and bowel function in female irritable bowel patients with alosetrin, a 5-HT_3 receptor antagonist. Aliment Pharmacol Ther 1999; 13:1149–59.

[11] Camilleri M, Chey WY, Mayer EA, Northcutt AR, Heath A, Dukes GE, et al. A randomized controlled clinical trial of the serotonin type 3 receptor antagonist alosetron in women with diarrhea-predominant irritable bowel syndrome. Arch Intern Med 2001;161:1733–40.

[12] Camilleri M, Northcutt AR, Kong S, Dukes GE, McSorley D, Mangel AW. Efficacy and safety of alosetron in women with irritable bowel syndrome: a randomized, placebo-controlled trial. Lancet 2000;355:1035–40.

[13] Lembo T, Wright RA, Bagby B, Decker C, Gordon S, Jhingran P, et al. Alosetron controls bowel urgency and provides global symptom improvement in women with diarrhea-predominant irritable bowel syndrome. Am J Gastroenterology 2001;96:2662–70.

[14] Jones RH, Holtmann G, Rodrigo L, Ensanullah RSB, Crompton PM, Jacques LA, et al. Alosetron relieves pain and improves bowel function compared with mebeverine in female nonconstipated irritable bowel syndrome patients. Aliment Pharmacol Ther 1999;13:1419–27.

[15] Miyata K, Kamato T, Nishida A, Katsuyama Y, Iwai A, Yuki H, et al. Pharmacologic profile of (R)-5-[(1-methyl-3-indolyl)carbonyl]-4,5,6,7-tetrahydro-1H- benzimidazole hydrochloride (YM060), a potent and selective 5-hydroxytryptamine 3 receptor antagonist, and its enantiomer in the isolated tissue. J Pharmacol Exp Ther 1991;259:15–21.

[16] Rabasseda X. Ramosetron, a 5-HT_3 receptor antagonist for the control of nausea and vomiting. Drugs Today (Barc) 2002;38:75–89.

[17] Miyata K, Kamato T, Nishida A, Ito H, Yuki H, Yamamo M, et al. Role of the serotonin 3 receptor in stress-induced defecation. J Pharmacol Exp Ther 1992;261:297–303.

[18] Miyata K, Ito H, Fukudo S. Involvement of the 5-HT_3 receptor in CRH-induced defecation in rats. Am J Physiol 1998;274:G827–31.

[19] Hirata T, Keto Y, Funatsu T, Sasamata M, Miyata K. Effects of ramosetron hydrochloride on defecation and abdominal pain in rats. Gastroenterology 2005;128 Suppl 2:A466.

[20] Matsueda K, Harasawa S, Hongo M, Hiwatashi N, Sasaki D. A Phase II trial of the novel serotonin type 3 receptor antagonist ramosetron in Japanese male and female patients with diarrhea-predominant irritable bowel syndrome. Under review.

[21] Camilleri M, Mangel AW, Fehnel SE, Drossman DA, Mayer EA, Talley NJ. Primary endpoints for irritable bowel syndrome trials: a review of performance of endpoints. Clin Gastroenterol Hepatol 2007;5:534–40.

[22] Chang L, Heitkemper MM. Gender differences in irritable bowel syndrome. Gastroenterology 2002;123:1686–701.

[23] Whitehead WE, Cheskin LJ, Heller BR, Robinson JC, Crowell MD, Benjamin C, et al. Evidence for exacerbation of irritable bowel syndrome during menses. Gastroenterology 1990;98:1485–9.

[24] Houghton LA, Lea R, Jackson N, Whorwell PJ. The menstrual cycle affects rectal sensitivity in patients with irritable bowel syndrome but not healthy volunteers. Gut 2002;50:471–4.

[25] Naliboff BD, Berman S, Chang L, Derbyshire SWG, Suyenobu B, Vogt BA, et al. Sex-related differences in IBS patients: central processing of visceral stimuli. Gastroenterology 2003;124:1738–47.

[26] US Food and Drug Administration Center for Drug Evaluation and Research, Lotronex Pharmacology Review(s), http:: //www.fda.gov/cder/foi/nda/2000/21107a_Lotronex.htm

[27] Berman S, Munakata J, Naliboff BD, Chang L, Mandelkern M, Silverman D, et al. Gender differences in regional brain response to visceral pressure in IBS patients. Eur J Pain 2000;4:157–72.

[28] Berman SM, Chang L, Suyenobu B, Derbyshire SW, Stains J, Fitzgerald L, et al. Condition-specific deactivation of brain regions by 5-HT_3 receptor antagonist alosetron. Gastroenterology 2002;123:969–77.

[29] Mawe GM, Coates MD, Moses PL. intestinal serotonin signalling in irritable bowel syndrome [review article]. Aliment Pharmacol Ther 2006;23:1067–76.

[30] Coates MD, Mahoney CR, Linden DR, Sampson JE, Chen J, Blaszyk H, et al. Molecular defects in mucosal serotonin content and decreased serotonin reuptake transporter in ulcerative colitis and irritable bowel syndrome. Gastroenterology 2004;126:1657–64.

[31] Yeo A, Boyd P, Lumsden S, Saunders T, Handley A, Stubbins M, et al. Association between a functional polymorphism in the serotonin transporter gene and diarrhoea predominant irritable bowel syndrome in women. Gut 2004; 53:1452–8.

[32] Camilleri M. Is there a SERT-a in association with IBS? Gut 2004;53:1396–9.

[33] Tally NJ, Zinsmeister AR, Melton LJ III. Irritable bowel syndrome in a community: symptom subgroups, risk factors, and health care utilization. Am J Epidemiol 1995;142:76–83.

[34] Lotronex® tablets (prescribing information/product label).

[35] Suh DC, Kahler KH, Choi IS, Shin H, Kralstein J, Shetzline M. Patients with irritable bowel syndrome or constipation have an increased risk for ischaemic colitis. Aliment Pharmacol Ther 2007;25:681–92.

BJCP British Journal of Clinical Pharmacology

DOI:10.1111/j.1365-2125.2008.03143.x

Brain histamine H_1 receptor occupancy of orally administered antihistamines, bepotastine and diphenhydramine, measured by PET with ^{11}C-doxepin

Manabu Tashiro,[1] Xudong Duan,[1] Motohisa Kato,[3] Masayasu Miyake,[1] Shoichi Watanuki,[1] Yoichi Ishikawa,[2] Yoshihito Funaki,[2] Ren Iwata,[2] Masatoshi Itoh[1] & Kazuhiko Yanai[1,3]

Divisions of [1]Cyclotron Nuclear Medicine and [2]Radiopharmaceutical Chemistry, Cyclotron and Radioisotope Centre, Tohoku University, and [3]Department of Pharmacology, Tohoku University Graduate School of Medicine, Sendai, Miyagi, Japan

Correspondence
Dr Manabu Tashiro, Division of Cyclotron Nuclear Medicine, Cyclotron and Radioisotope Centre, Tohoku University, 6-3 Aoba, Aramaki, Aoba-ku, Sendai, Miyagi 980-8578, Japan.
Tel: + 81 22 795 7797
Fax: + 81 22 795 7797
E-mail: mtashiro@m.tains.tohoku.ac.jp

Keywords
first-generation antihistamine, histamine H_1 receptor occupancy, placebo-controlled crossover study design, positron emission tomography, second-generation antihistamine

Received
3 April 2007

Accepted
17 January 2008

Published *OnlineEarly*
11 April 2008

WHAT IS ALREADY KNOWN ABOUT THIS SUBJECT

- 'Bepotastine besilate' is a novel second-generation antihistamine developed in Japan and its antiallergic effects have already been demonstrated by various studies.
- However, only a few clinical studies regarding its sedative property are available.
- In addition, histamine H_1 receptor occupancy (H_1RO) of this new antihistamine has never been measured by positron emission tomography (PET).

WHAT THIS STUDY ADDS

- This paper provides the first measurement result of cerebral H_1RO of bepotastine besilate (approximately 15%) as determined by PET.
- This result is in accordance with the clinical classification of bepotastine as a second-generation antihistamine.
- In addition, the relationship between subjective sleepiness and cerebral H_1RO of this second-generation antihistamine is demonstrated for the first time using a placebo-controlled crossover study design.

AIMS

Antihistamines are frequently used for treating various allergic diseases, but often induce sedation. The degree of sedation can be evaluated by measuring histamine H_1 receptor occupancy (H_1RO) in the brain using positron emission tomography (PET). The aim was to measure H_1RO of bepotastine, a new second-generation antihistamine, and to compare it with that of diphenhydramine.

METHODS

Eight healthy male volunteers (mean age ± SD 24.4 ± 3.3 years) were studied after single oral administration of bepotastine (10 mg), diphenhydramine (30 mg) or placebo, by PET imaging with ^{11}C-doxepin in a crossover study design. Binding potential ratio and H_1ROs were calculated using placebo data and were compared between bepotastine and diphenhydramine in the anterior and posterior cingulate gyri (ACG and PCG, respectively), superior and inferior frontal cortices (SFC and IFC, respectively), orbitofrontal cortex (OFC), insular cortex (IC), lateral and medial temporal cortices (LTC and MTC, respectively), parietal cortex (PC), occipital cortex (OC) and sensorimotor cortex (SMC). Plasma concentration of each antihistamine was measured, and its correlation to H_1RO was examined.

RESULTS

H_1RO after bepotastine treatment was significantly lower than that after diphenhydramine treatment in all cortical regions ($P < 0.001$). Mean H_1ROs of bepotastine and diphenhydramine were 14.7% and 56.4%, respectively. H_1ROs of both bepotastine and diphenhydramine correlated to their respective drug plasma concentration ($P < 0.001$).

CONCLUSION

Oral bepotastine (10 mg), with its relatively low H_1RO and thus minimal sedation, has the potential for use as a mildly or slightly sedative antihistamine in the treatment of various allergic disorders.

Introduction

Histamine H_1 receptor (H_1R) antagonists, or antihistamines, are often used for treating allergic disorders such as seasonal rhinitis. Antihistamines mainly act on peripheral tissues, but can induce sedation as a central side-effect. This undesirable side-effect is caused by blockade of nerve transmission in the histaminergic neuron system which projects from the tuberomammillary nucleus in the posterior hypothalamus to almost all cortical areas [1–5]. First-generation antihistamines that can easily penetrate the blood–brain barrier (BBB), such as diphenhydramine and d-chlorpheniramine, tend to occupy a large proportion of postsynaptic H_1Rs as demonstrated by positron emission tomography (PET) [1, 6–8]. PET also reveals that second-generation antihistamines (mildly or slightly sedative antihistamines), such as cetirizine and olopatadine, can slightly penetrate the BBB and occupy some H_1Rs [1, 6, 9, 10]. Users who take these second-generation antihistamines at doubled or tripled doses to achieve desired effects may suffer from dose-related cognitive impairment. Third-generation antihistamines (truly nonsedative antihistamines), such as fexofenadine and ebastine, hardly penetrate the BBB and do not occupy H_1Rs even at high doses, as demonstrated by ^{11}C-doxepin PET [9]. Thus, the sedative property of antihistamines can be evaluated in terms of H_1R occupancy (H_1RO). Such variations in BBB permeability are caused by various factors, including differences in lipophilicity, molecular size and actions of drug transporters.

Bepotastine besilate ({d-(S)-4-[4-[(4-chlorophenyl)(2-pyridyl)methoxy]piperidino} butyric acid monobenzenesulphonate, betotastine besilate, CAS 125602-71-3, TAU-284 or Talion), a new second-generation antihistamine developed in Japan, is now used as an oral tablet for allergic rhinitis and chronic urticaria (Figure 1) [11–13]. Previous studies have demonstrated its excellent antiallergic effects compared with other antihistamines such as ketotifen, cetirizine, epinastine and terfenadine [14–18], whereas only a few studies have shown its central effects [18, 19]. Only one available animal behavioural study by Kato and colleagues has demonstrated that bepotastine is a highly specific drug to H_1R, having no significant binding affinity for histamine H_3, adrenergic α_1, α_2, β, dopaminergic D_2, serotonergic $5HT_2$, muscarinic or benzodiazepine receptors, and

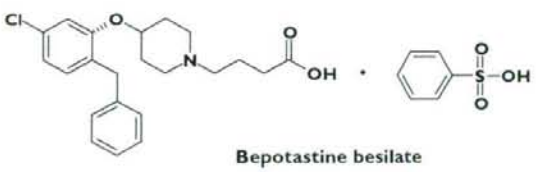

Bepotastine besilate

Figure 1
Chemical structure of bepotastine besilate

that it poorly penetrates the BBB [19]. Takahashi and colleagues first conducted a double-blind, placebo-controlled, crossover study to measure subjective sedation and psychomotor activities following administration of bepotastine, cetirizine, fexofenadine and olopatadine [18], where bepotastine had the least sedative effect [18].

To date, we have measured H_1ROs of various second-generation and third-generation antihistamines, but not that of bepotastine. It is of great interest to examine H_1RO of bepotastine in humans. Thus, the primary aim of the present study was to measure subjective sedation and cerebral H_1RO of bepotastine and to compare the results with those of diphenhydramine, a typical sedative antihistamine [20], using a placebo-controlled crossover study design that would make the interpretation of results clearer and easier by minimizing potential errors due to intersubject variability [10]. Another aim was to determine whether bepotastine should be classified as a truly nonsedative or mildly sedative antihistamine.

Methods

The present study was approved by the Committee on Clinical Investigation at Tohoku University Graduate School of Medicine, Japan, and was performed in accordance with the principles of the Declaration of Helsinki. All experiments were performed at the Cyclotron and Radioisotope Centre, Tohoku University.

Subjects and study design

Eight male Japanese volunteers (mean age ± SD 24.4 ± 3.3 years), who provided written informed consent after receiving a detailed description of the study, were recruited. All subjects were in good health with no clinical history of major physical or mental illness, showed no abnormality in brain magnetic resonance imaging (MRI), and were not receiving any concomitant medication likely to interfere with the study results. Nicotine, caffeine, grapefruit and grapefruit juice were not allowed on the test day, and alcohol was not allowed on the test day or the day before PET measurement.

All subjects underwent PET measurement after single oral administration of bepotastine (10 mg), diphenhydramine (30 mg) or a lactobacteria preparation (6 mg) used as placebo in a three-way crossover study, with minimum wash-out intervals of 7 days between treatments. The lactobacteria preparation has been widely used as placebo in Japan, and its administration has produced no statistical difference between pre- and post-administration in previous cognitive studies [7, 9, 10, 21]. The present PET study was conducted in a single-blinded manner, and after drug administration each subject was asked to remain seated comfortably on a sofa. To determine bepotastine and diphenhydramine plasma concentrations, blood samples were collected from each subject

before drug administration and at 0, 60, 120 and 180 min post administration. Subjective sleepiness of each subject was also measured at 0, 60, 120 and 180 min post administration using the Line Analogue Rating Scale (LARS) [22] and the Stanford Sleepiness Scale (SSS) as used in previous studies [9, 23].

Measurement of plasma concentrations of bepotastine and diphenhydramine

Plasma concentrations of bepotastine and diphenhydramine were measured using liquid chromatography/tandem mass spectrometry (LC/MS/MS) together with an electrospray ionization method [24]. LC was performed on an Agilent 1100 Series LC instrument (Agilent Technologies Inc., Santa Clara, CA, USA) equipped with an analytical column. The MS/MS system was the API 4000 (Applied Biosystems/MDS Sciex, ON, Canada). The Solid Phase Extraction (SPE) cartridge (OASIS HLB 3 ml/60 mg; Waters Corp., Milford, MA, USA) was pretreated with 2 ml of methanol, 2 ml of water and 2 ml of 0.2 M Na_2CO_3/HCl buffer (pH 11).

For measurement, an internal standard solution (10 μl) and methanol (10 μl) were added to each plasma sample (50 μl). To the resulting solution, 930 ml of 0.2 M Na_2CO_3/HCl buffer was added for bepotastine measurement, and 1000 μl of 0.1% formic acid containing acetonitrile/methanol (50 : 50, v/v) was added for diphenhydramine measurement. The mixture was applied onto the SPE cartridge after pretreatment as mentioned above. Separations were carried out on a high-performance liquid chromatography (HPLC) column [CAPCELL PAK C18 MG II (3 μm) 2.0 mmϕ × 100 mm; Shiseido Co., Ltd, Tokyo, Japan) at a flow rate of 0.2 ml min^{-1} and at a column temperature of 40 °C. The reconstituted extract (5 μl) was injected onto an HPLC system with mobile phases for bepotastine measurement including 10 mmol l^{-1} ammonium acetate and acetonitrile of varied concentrations, namely, 32% (0–9 min), 70% (9.5–12.5 min) and 32% (12.6–24 min), and with mobile phases for diphenhydramine measurement including 0.1% heptafluorobutyric acid and acetonitrile of varied concentrations, namely, 40% (0–7 min), 70% (7.5–10.5 min) and 40% (11–21 min).

Detection of bepotastine was based on fragmentation of the precursor ion (m/z = 389 to product ion m/z = 202 with collision energy of 29 eV for bepotastine, and m/z = 256 to product ion m/z = 167 with collision energy of 19 eV for diphenhydramine), and that of the internal standard was based on fragmentation of the precursor ion (m/z = 389 to product ion m/z = 201 with collision energy of 29 eV for bepotastine, and m/z = 270 to product ion m/z = 181 with collision energy of 17 eV for diphenhydramine) in positive multiple reaction monitoring (MRM) mode. Positive ions were detected using an API 4000 system at 550 °C nebulizer gas temperature, with 5000 V ion spray voltage, 68.9 kPa (nitrogen) curtain gas and Level 4 collision gas for bepotastine, and 206.8 kPa curtain gas and Level 4 collision gas for diphenhydramine. Chromatographic data for positive MRM were collected using Analyst software (ver. 1.2, Applied Biosystems/MDS Sciex) with cycle times of 1.010 s per cycle for bepotastine and 0.5200 s per cycle for diphenhydramine. The lowest detectable concentration was around 1 ng ml^{-1} for both antihistamines, and some values slightly under the threshold (only for diphenhydramine) were extrapolated. As for validation, the following items were checked for bepotastine and diphenhydramine, respectively: accuracy (100.7% and 102.2%), correlation coefficients to standard solutions ($r > 0.99$ for both), and coefficients of variation (CVs) of three different concentrations ($n = 5$) (1.7–2.3%, 1.8–3.8%).

For examination of the relationship between estimated binding potential ratio (BPR) of ^{11}C-doxepin and plasma concentration of each antihistamine, the areas under the curves (AUCs) of bepotastine and diphenhydramine were calculated for 0–180 min ($AUC_{0-3\,h}$) post administration (Table 1).

PET tracer and image acquisition

Doxepin is one of the tricyclic antidepressants that has binding affinity to other receptors such as muscarinic receptors to some extent. However, its affinity to histamine H_1Rs is much higher than to other receptors and is very high compared with other antidepressants [25]. Thus, doxepin's affinity to other receptor systems is negligible in this

Table 1

Plasma concentrations of bepotastine and diphenhydramine ($n = 8$)

Bepotastine time (min)	Mean (ng ml^{-1})	SEM	CV, %	Diphenhydramine time (min)	Mean (ng ml^{-1})	SEM	CV, %
0	0.0	0.0	**0.0**	0	0.0	0.0	**0.0**
60	78.0	17.3	**62.9**	60	6.2	2.3	**104.4**
120	71.0	4.6	**18.2**	120	16.3	2.1	**36.4**
180	82.6	8.4	**28.7**	180	19.7	1.2	**17.0**
$AUC_{0-3\,h}$	196.1	24.3	**35.0**	$AUC_{0-3\,h}$	32.3	4.0	**35.3**

CV, coefficient of variation; SEM, standard error of mean.

imaging study, as also confirmed by experiments using histamine H_1R knock-out mice, where doxepin binding in the brain was nearly zero [26]. Thereafter, ^{11}C-doxepin has been used to evaluate the distribution of histamine H_1Rs. ^{11}C-doxepin kinetics in plasma and the brain are not affected by the sedative antihistamine d-chlorpheniramine using arterial sampling data combined with metabolite analysis [6].

In the present study, ^{11}C-doxepin was prepared by ^{11}C-methylation of desmethyl doxepin with ^{11}C-methyl triflate as described previously [10, 27]. ^{11}C-doxepin radiochemical purity was >99%, and its specific radioactivity at the time of injection was 120.9 ± 80.55 GBq μmol^{-1} (3268 ± 2177 mCi μmol^{-1}). ^{11}C-doxepin-containing saline solution was intravenously injected into each subject at 90 min post administration, a time close to T_{max} of both antihistamines (1.2 h for bepotastine and 2–3 h for diphenhydramine). The injected dose and cold mass of ^{11}C-doxepin were 135.4 ± 19.83 MBq (3.660 ± 0.536 mCi) and 1.587 ± 0.895 nmol, respectively, and the radiological dose was calculated based on a previous study on radiological exposure [28].

Approximately 60 min after ^{11}C-doxepin injection, the subjects were positioned on the coach of the PET scanner (SET2400W; Shimadzu Co., Kyoto, Japan) for transmission scan (6 min) and emission scan in the three-dimensional (3D) mode lasting for 15 min (70–85 min post injection of ^{11}C-doxepin) in a similar fashion to our previous work [10, 29]. PET brain images from a 15-min-long emission scan were corrected for scattering based on a previous study [30] and for tissue attenuation using post-injection transmission scan data according to previous work [31]. Brain images were reconstructed with a filtered back-projection algorithm, with the aid of a supercomputer SX-7 at the Information Synergy Centre, Tohoku University, Sendai, Japan. The brain images were then normalized by plasma radioactivity at 10 min post injection to yield images reflecting distribution volume (DV) based on our static scan protocol reported previously [10, 32]. Validation using venous sampling instead of arterial sampling was carried out by another group, giving no difference between venous and arterial sampling at 10 min post injection (M. Senda, personal communication, 23 August 2007).

Three brain images of each subject, following oral administration of bepotastine, diphenhydramine and placebo, were coregistered to an identical stereotaxic brain coordinate system using an MRI-T1 image of each subject, with the aid of Statistical Parametric Mapping (SPM2, Wellcome Department, UK) software package [33]. MRI images were obtained with a 1.5-T magnetic resonance (MR) scanner (HiSpeed, Ver. 9.1; General Electric Inc., WI, USA) at Sendai Seiryo Clinic (miyagi, Japan). T1-weighted images (Vascular TOF SPGR: TR/TE 50/2.4 ms, FA 45°, number of excitations 1, matrix size 256 × 256, spatial resolution: x, y, z = 0.86, 0.86, 20.0 mm, respectively) were collected from all subjects.

Regions of interest (ROIs) were first placed on the following brain regions on the T1 images that had precise anatomical information, i.e. anterior and posterior cingulate gyri (ACG and PCG, respectively), prefrontal cortices (PFC), orbitofrontal cortex (OFC), insular cortex (IC), temporal cortex (TC), parietal cortex (PC), occipital cortex (OC), primary sensorimotor cortex (SMC), thalamus, striatum, midbrain, pons, and cerebellum. ROI was defined for each cortical region by two to five circles with a diameter of 7.6 mm for each hemisphere in four to five consecutive brain transaxial slices, as indicated in Figure 2A. For the thalamus, striatum, pons and midbrain, the margin of each region was traced in MRI T1 images. An averaged value from all ROIs was used as a representative value of each region. Information on ROI location was automatically transferred to the coregistered three PET images reflecting DV, and the binding potential ratio (BPR) was calculated for each region using the following equation: BPR = [(DV of each region − DV of cerebellum)/DV of cerebellum] [8, 9]. Finally, H_1ROs of bepotastine and diphenhydramine were calculated for each cortical region using the following equation: H_1RO = [(BPR of placebo − BPR of antihistamine)/BPR of placebo] × 100. BPR brain images were also created by applying the same equation to each DV brain image [8–10, 34, 35]. BPR brain images were analysed statistically on a voxel-by-voxel basis using SPM2 [33], following spatial normalization and smoothing using the same method as in our previous work. Differences in parameter values between bepotastine, diphenhydramine and placebo (control) were statistically examined, and regional maxima of statistical significance ($P < 0.001$) were projected onto surface-rendered MRI-T1 standard brain images. Precise locations of statistically significant regions were identified with the Co-Planar Stereotaxic Atlas [36].

Statistical analysis

Differences in subjective sleepiness and BPR between bepotastine, diphenhydramine and placebo were examined using ANOVA followed by multiple comparison with Bonferroni correction. The difference in H_1RO between bepotastine and diphenhydramine was examined using paired Student's *t*-test. The relationship between plasma drug concentration (AUC) and H_1RO was examined using Pearson's correlation test. A probability of $P < 0.05$ was considered statistically significant. All statistical examinations were performed using SPSS for Windows 13.0.1 (Japanese version).

Results

Plasma concentrations of bepotastine and diphenhydramine

Mean plasma concentrations and AUCs of bepotastine and diphenhydramine are shown in Table 1. The peak mean

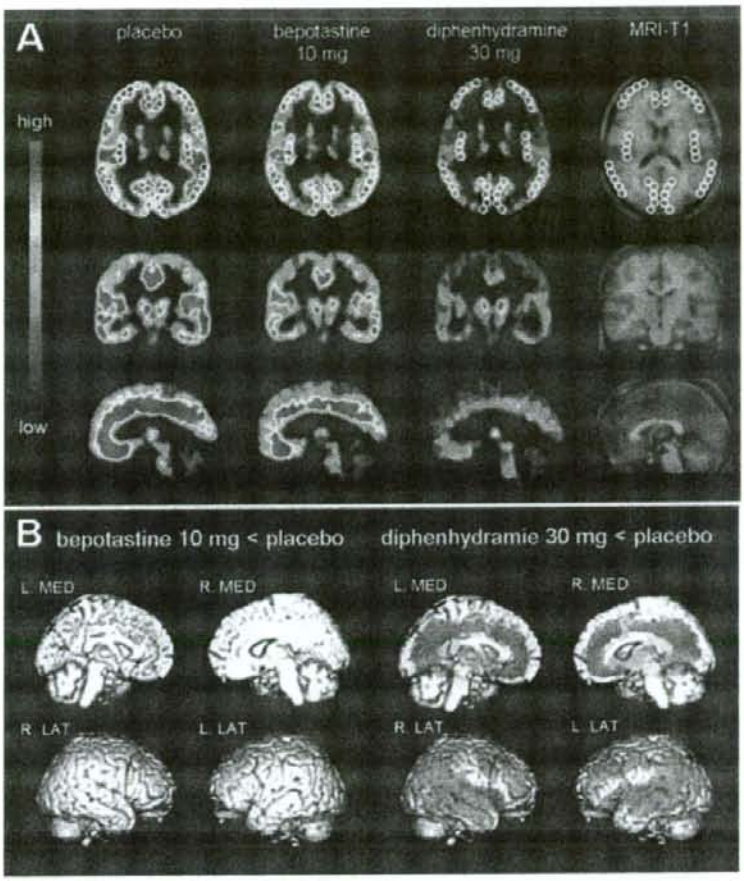

Figure 2

Binding potential ratio (BPR) images of ^{11}C-doxepin in the human brain (A) and results of voxel-by-voxel comparison (B). BPR of ^{11}C-doxepin was calculated in healthy male subjects ($n = 8$) by positron emission tomography following oral administrations of placebo (left), bepotastine (10 mg, middle) or diphenhydramine (30 mg, right), and their magnetic resonance imaging-T1 images (far right), demonstrated in the transaxial (top), coronal (middle) and sagittal (bottom) sections for each treatment condition, were compared (A). White circles in the transaxial images indicate the regions of interest (ROIs). The brain image of each subject was transformed to fit stereotaxic brain space (spatial normalization) and was averaged across each drug condition to generate the mean images displayed (A). The images demonstrate that diphenhydramine treatment results in BPR significantly lower than those of other drug conditions (B). Height threshold of voxel values was set at $P < 0.001$ and extent threshold was set at 10 voxel minimum. Results were not corrected for multiple comparisons. There are no areas with significantly lower BPR after bepotastine treatment compared with those after placebo treatment ('bepotastine 10 mg < placebo' in the left columns). In contrast, red colour shows areas with significantly lower BPR after diphenhydramine treatment compared with those after placebo treatment ('diphenhydramine 30 mg < placebo' in the right columns). In both columns, significant areas are demonstrated in four aspects, namely, left and right medial (L. MED and R. MED) and right and left lateral (R. LAT and L. LAT) aspects ($P < 0.001$, uncorrected, using SPM2) (B)

plasma concentration of bepotastine ranged from 60 to 180 min post administration because, in five of the eight subjects, it peaked at 60 min post administration, whereas in the other three subjects it peaked at 120 or 180 min post administration. Mean plasma concentration of diphenhydramine was maximal from 120 to 180 min post administration (Table 1).

Subjective sleepiness

Results of mean subjective sleepiness are shown in Figure 3. Mean subjective sleepiness of diphenhydramine peaked at 120–180 min post administration and that of bepotastine at 120 min post administration. Both LARS and SSS manifested similar patterns. Multiple comparison

following repeated ANOVA demonstrated that subjective sleepiness following diphenhydramine administration was significantly stronger ($P < 0.001$) than that of both bepotastine and placebo at 120 and 180 min post administration, and that of bepotastine was not significantly different from that of placebo (Figure 3).

Brain distribution of ^{11}C-doxepin

Radioactivity distribution patterns of ^{11}C-doxepin are shown in Figure 2A. The mean BPR image, averaged from eight subjects, following bepotastine treatment was similar to that following placebo treatment in an individual subject. Namely, high radioactivity was observed in ACG, PCG, PFC, OFC, IC, TC, PC, OC and SMC following both treatments, whereas the radioactivity distribution pattern following diphenhydramine treatment was much lower than that following the other two treatments (Figure 2A).

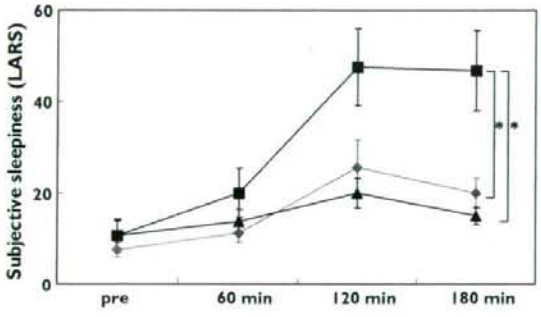

Figure 3

Subjective sleepiness evaluated using the Line Analogue Rating Scale (LARS). Eight healthy subjects were studied following oral administration of bepotastine (BEP, 10 mg), diphenhydramine (DIP, 30 mg) or placebo (PLA). *$P < 0.001$ by ANOVA followed by multiple comparison with Bonferroni correction. Error bars represent interindividual variability (SEM). BEP, (◆); DIP, (■); PLA, (▲)

Comparison of parametric BPR images (bepotastine vs. diphenhydramine)

Using SPM2 on a voxel-by-voxel basis, parametric brain BPR images following bepotastine or diphenhydramine treatment were statistically compared with those following placebo treatment. In Figure 2B, red areas show brain regions where BPRs were significantly lower ($P < 0.001$) following diphenhydramine treatment than those following placebo treatment (Figure 2B, right; Table 3). ACG, PFC and TC demonstrated significantly lower BPR after diphenhydramine treatment than after placebo treatment (Table 2). On the other hand, SPM analysis showed no brain areas where BPR was significantly lower after bepotastine treatment than after placebo treatment (Figure 2B, left).

ROI-based comparison of BPR and H_1RO

BPRs in H_1R-rich regions such as ACG, PFC, IC, TC, PC and OC were evaluated based on ROI analysis (Figure 4A). BPRs following bepotastine treatment were only slightly different from those following placebo treatment. However, BPRs following diphenhydramine treatment were significantly lower than those following placebo or bepotastine treatment ($P < 0.001$) for all cortical regions. In the thalamus, striatum, pons and midbrain, there was no significant difference in BPRs between diphenhydramine, bepotastine and placebo treatments.

H_1RO following diphenhydramine or bepotastine treatment was also calculated using H_1RO after placebo treatment as baseline (0%) (Figure 4B). Cortical mean H_1RO following bepotastine treatment was approximately 14.7% and that following diphenhydramine treatment was approximately 56.4%. H_1ROs following bepotastine treatment were significantly lower than those following diphenhydramine treatment ($P < 0.001$) in all cortical

Table 2

Binding potential ratios and histamine H_1 receptor occupancies in placebo, bepotastine and diphenhydramine conditions

Regions	BPR_{Pla} Mean	SD	BPR_{BEP} Mean	SD	BPR_{DIP} Mean	SD	95% CI Pla-DIP	BEP-DIP	H_1RO_{BEP} Mean	SD	H_1RO_{DIP} Mean	SD	95% CI DIP-BEP	C.E. BEP	C.E. DIP
Anterior cingulate gyrus (ACG)	0.78	0.22	0.66	0.11	0.33	0.09	0.28, 0.64	0.24–0.42	14.3	11.9	57.7	8.9	33.1, 53.8	0.54	−0.30
Posterior cingulate gyrus (PCG)	0.85	0.18	0.71	0.09	0.40	0.09	0.28, 0.61	0.18–0.43	14.8	12.3	52.0	9.7	24.1, 50.2	0.51	−0.57
Prefrontal cortex (PFC)	0.65	0.16	0.55	0.10	0.27	0.10	0.26, 0.51	0.20–0.37	14.2	12.2	59.3	12.2	31.7, 58.5	0.66	−0.28
Orbitofrontal cortex (OFC)	0.60	0.20	0.50	0.13	0.24	0.08	0.23, 0.51	0.18–0.35	15.4	11.8	60.5	6.9	34.1, 56.2	−0.01	−0.28
Insular cortex (IC)	0.80	0.18	0.66	0.09	0.36	0.09	0.29, 0.57	0.21–0.37	15.9	9.9	54.0	8.0	28.7, 47.4	0.52	−0.29
Temporal cortex (TC)	0.61	0.18	0.51	0.09	0.27	0.11	0.22, 0.48	0.21–0.28	14.4	12.6	57.2	11.0	30.6, 55.0	0.04	−0.20
Parietal cortex (PC)	0.54	0.17	0.44	0.13	0.21	0.12	0.22, 0.43	0.17–0.30	16.0	16.9	62.8	16.5	30.6, 62.9	0.34	0.16
Occipital cortex (OC)	0.49	0.10	0.43	0.06	0.27	0.08	0.15, 0.31	0.11–0.22	11.0	12.8	46.3	13.5	23.5, 47.0	0.31	0.06
Somatosensory cortex (SMC)	0.44	0.14	0.36	0.10	0.19	0.09	0.13, 0.38	0.06–0.29	16.5	15.9	57.6	21.6	18.9, 63.3	0.78	−0.18
Mean	0.64	0.14	0.54	0.12	0.28	0.07			14.7	1.6	56.4	5.0		0.48	−0.19

Results of statistical evaluation (*P*-values) are shown in Figure 3. BEP, bepotastine; BPR, binding potential ratio; C.E., correlation efficient of H_1 RO to plasma concentration of each antihistamine; 95% CI, 95% confidence interval; DIP, diphenhydramine; H_1RO, histamine H_1 receptor occupancy; Pla, placebo; SD, standard deviation.

Table 3

Regions with significantly lower specific binding following diphenhydramine treatment compared with those following placebo treatment

Regions	Brodmann's area	Hemisphere	x, y, z (mm)	Cluster size	*T*-value	*Z*-value	*P*-value
Superior temporal gyrus	22	R	54–56 16	29 543	11.55	6.41	<0.001
Medial temporal gyrus	21	L	–58-12-12	S.C.	11.41	6.37	<0.001
Precuneus	7	R	26–58 48	S.C.	11.08	6.29	<0.001
Medial temporal gyrus	21	L	–48 4–32	32	8.14	5.41	<0.001
Superior frontal gyrus	10	L	–24 60 12	104	7.53	5.18	<0.001
Superior frontal gyrus	8	L	–28 24 50	38	7.07	5	<0.001
Medial frontal gyrus	10	R	28 54 14	1342	8.53	5.55	<0.001
Medial frontal gyrus	9	R	42 6 40	S.C.	8.46	5.52	<0.001
Medial frontal gyrus	6	R	24 4 58	S.C.	8.98	5.7	<0.001
Inferior frontal gyrus	46	L	–40 44 12	38	8.96	5.69	<0.001

Cluster size is represented by the number of voxels (voxel size: 2.0 × 2.0 × 2.0 mm^3). S.C., the same cluster as above. Results are not corrected for multiple comparisons.

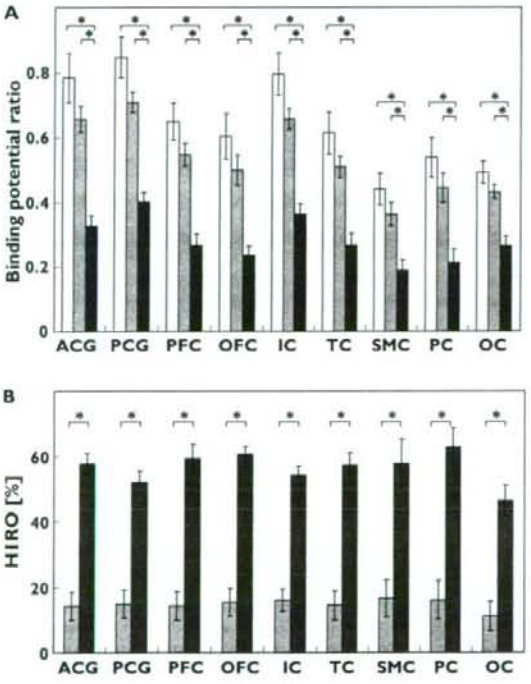

Figure 4

Region of interest (ROI)-based analyses of binding potential ratios (BPR) (A) and histamine H_1 receptor occupancy (H_1RO) (B) in the cortex. ROI measurements were performed in the anterior and posterior cingulate gyri (ACG and PCG, respectively), prefrontal cortex (PFC), orbitofrontal cortex (OFC), insular cortex (IC), temporal cortex (TC), sensorimotor cortex (SMC), parietal cortex (PC) and occipital cortex (OC) after treatments with placebo (PLA), bepotastine (BEP) and diphenhydramine (DIP). Comparison of BPRs shows differences in the sedative properties of the three drugs (A). H_1ROs due to BEP and DIP are shown, taking H_1RO due to placebo as 0% (B). *$P < 0.001$, ANOVA followed by multiple comparison with Bonferroni correction. Error bars represent interindividual variability (SEM). PLA, (□); BEP, (▨); DIP, (■)

regions. These data demonstrate that BPR following bepotastine treatment is substantially higher than that following diphenhydramine treatment in all cortical regions studied.

Relationships between subjective sleepiness, plasma drug concentration and H_1RO

Subjective sleepiness (AUC of LARS curve) did not significantly correlate to plasma concentration of bepotastine ($r = 0.04$), but did correlate well to plasma concentration of diphenhydramine ($r = 0.72$). H_1ROs following bepotastine administration significantly correlated to plasma concentration of bepotastine in ACG, PCG, PFC, IC and SMC, whereas those following diphenhydramine administration were all negatively correlated (Table 2). A similar trend was observed between cortical mean H_1RO and plasma concentration of both antihistamines (Figure 5A,B). However, when the baseline data are plotted together, mean H_1RO due to diphenhydramine tended to increase rapidly with diphenhydramine concentration, whereas that due to bepotastine gradually increased with bepotastine concentration (Figure 5A,B). H_1RO following bepotastine administration did not significantly correlate to subjective sleepiness ($r = 0.01$) (Figure 5D), whereas that following diphenhydramine administration negatively correlated to subjective sleepiness when the baseline data were plotted together (Figure 5C).

Discussion

Recently, molecular imaging techniques have been actively applied in clinical pharmacology research [1, 8–10, 37]. One of the primary aims of such work is to evaluate the relationship between doses of therapeutic drugs and their adverse reactions in terms of changes in 'endophenotypes' in the brain [38]. The primary aim of the present study was to clarify whether bepotastine belongs to second-generation antihistamines in terms of H_1RO. Another aim

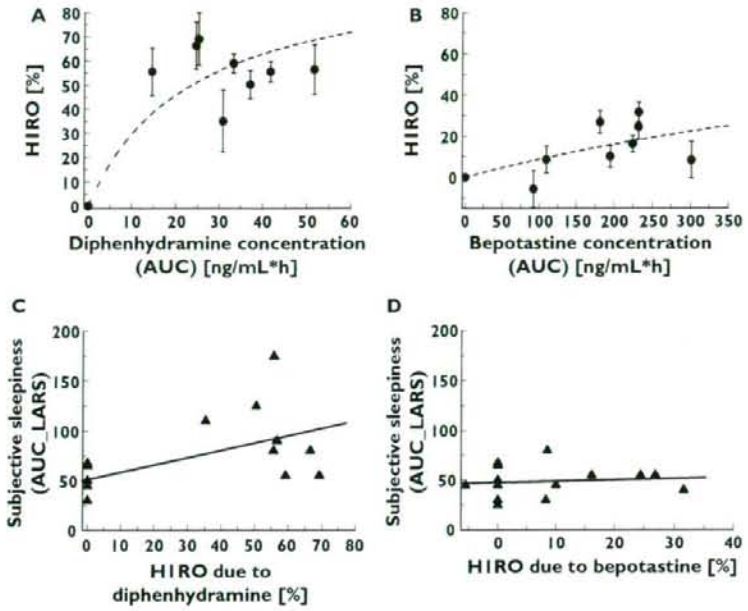

Figure 5

Relationship between mean H_1 receptor occupancy (H_1RO), plasma concentration and subjective sleepiness following administrations of bepotastine and diphenhydramine. Relationship between mean H_1RO (across brain regions) and plasma concentrations was examined for diphenhydramine (A) and bepotastine (B). Plasma concentrations of the two antihistamines are presented as area under the curve (AUC). H_1RO of diphenhydramine rapidly increases with plasma concentration, whereas H_1RO of bepotastine gradually increases with plasma concentration. Error bars represent intraindividual variability (SD). Dotted curves reflect the estimated curves of relationship between plasma concentration and the H_1RO analysed by the Michaelis–Menten equation (A and B). Subjective sleepiness (presented as AUC of line-analogue rating scale curve: AUC_LARS) demonstrates mild correlation to mean H_1RO due to diphenhydramine (C), whereas subjective sleepiness due to bepotastine demonstrates no correlation to mean H_1RO due to bepotastine (D)

was to determine whether bepotastine should be classified as a truly nonsedative or mildly sedative antihistamine, as previously discussed in the Consensus Group on New Generation Antihistamines (CONGA) [3].

In the present study, H_1ROs following a single oral administration of bepotastine (10 mg) or diphenhydramine (30 mg) were 14.7 and 56.4%, respectively. The relatively high H_1RO due to diphenhydramine agrees with those of other reported first-generation antihistamines [1, 6, 38]. Single oral administration of d-chlorpheniramine (2 mg) achieved 50–77% H_1RO, and this high H_1RO was associated with high prevalence of sleepiness and cognitive decline [6, 8, 39]. On the other hand, bepotastine's low H_1RO value suggests that this antihistamine can be classified into the category of second-generation antihistamines [6, 8, 9, 39–42, 38].

Thus, whether bepotastine can be classified as truly nonsedative or not is an additional point of clinical importance. In the present study, subjective sleepiness following bepotastine administration (10 mg) was negligible (Figure 3). This finding seems to be in accordance with that of Takahashi and colleagues [18], where bepotastine (10 mg) induced slight subjective sedation among healthy volunteers. In their study, the best performance was achieved following bepotastine treatment in a word-processing task compared with those following cetirizine (10 mg), fexofenadine (60 mg) or olopatadine (5 mg) treatment [18]. Another study [11] has demonstrated that results of serial arithmetic tests following oral administration of bepotastine (2.5, 5, 10 and 20 mg) showed no significant differences from those following placebo treatment. These clinical studies tried to demonstrate the nonsedative property of bepotastine, but they failed to include an active placebo (sedative antihistamine) to prove sensitivity of the selected tasks as recommended in the CONGA guideline [3]. An additional animal study [19] has demonstrated that bepotastine manifested a sedative profile similar to that of cetirizine and terfenadine. As a whole, these results suggest the low liability of bepotastine to produce sedative side-effects at a therapeutic dose of 10 mg. Considering the significant correlation between H_1RO and plasma drug concentration (AUC) found in the present study (Figure 5B), bepotastine may be classified as a mildly sedative antihistamine.

In general, H_1RO is used as an index of BBB permeability, but it could also be affected by gut absorption that can raise plasma drug concentration. At the molecular level, variation in BBB permeability has been determined by factors such as lipophilicity, molecular size and different actions of various drug transporters including P-glycoprotein (P-gp), an efflux pump expressed in capillary endothelial cells in the BBB [10]. Many lipophilic first-generation antihistamines are absorbed in full amount in the gut and can freely enter the brain tissue, whereas gut absorption and brain penetration of second-generation antihistamines tend to be reduced. For fexofenadine, a substrate of P-gp, both gut absorption and BBB permeability are highly reduced because of its low membrane permeability and high action of P-gp. For bepotastine, also a substrate of P-gp, the same extent of reduction as that of fexofenadine is observed [43]. The gradual increase in H_1RO with plasma bepotastine concentration, suggesting its relatively high membrane permeability (Figure 5B), may be associated with the action of P-gp in the BBB. On the other hand, gut absorption of bepotastine tends to be much higher than that of fexofenadine, presumably because of bepotastine's higher membrane permeability in the upper part of the small intestine where P-gp expression is low [43]. Such difference is one of the possible reasons for explaining the difference between bepotastine and fexofenadine. Another reason is that fexofenadine is transported not only by P-gp but also by the organic anion protein transporter family, further reducing its absorption in the gut [44, 45].

The limitations of the present method are as follows. The short scanning PET protocol would be useful especially in conducting a placebo-controlled crossover study because of the enormous mental and physical stress of volunteers observed in a previous study, where they were requested to complete four sets of 100-min-long PET examinations [34]. It is therefore important to develop a short scan protocol, although such protocols would include a larger amount of noise. Users of the PET system should consider these limitations. We note here that not exact values but, rather, approximations of DV and BP were measured in this study.

We were interested in the effects of an acute single dose of an antihistamine, and we planned to start PET scanning at the time point near T_{max} for each drug, but the tracer injection for diphenhydramine condition seemed to be slightly early since the plasma concentration of diphenhydramine was still increasing (Table 1). Therefore, H_1RO due to diphenhydramine might give slightly different values when measured in the equilibrium state. This might be the reason why H_1RO following diphenhydramine treatment did not correlate positively to the plasma concentration of diphenhydramine, contrary to our expectation based on a previous study using d-chlorpheniramine [8].

In summary, we have examined H_1RO of bepotastine (10 mg; 14.7%) and compared it with that of diphenhydramine (30 mg; 56.4%) given as a single oral administration, using PET in a placebo-controlled crossover study. It is suggested that oral administration of bepotastine (10 mg), with its low H_1RO and minimal sedation effects, is useful for treating various allergic disorders. As for the dose dependency of its sedative effects, another cognitive study involving an active placebo is needed in order to draw a definitive conclusion. The dose dependency of H_1RO should also be examined by PET measurements at higher doses.

This work was in part supported by Grants-in-Aid for Scientific Research (nos. 17390156 for K.Y. and 16790308 for M.T.) from the Japan Society of Promotion of Science (JSPS) and the Ministry of Education, Culture, Sports, Science and Technology in Japan, as well as by a grant from the Japan Society of Technology (JST) on research and education in 'molecular imaging'. We thank the volunteers of the PET study and Mrs Kazuko Takeda for her care of them. We also thank TANABE R&D SERVICE Co., Ltd (Osaka, Japan) for technical support in measuring the plasma concentration of antihistamines.

REFERENCES

1 Yanai K, Tashiro M. The physiological and pathophysiological roles of neuronal histamine: an insight from human positron emission tomography studies. Pharmacol Ther 2007; 113: 1–15.

2 Haas H, Panula P. The role of histamine and the tuberomamillary nucleus in the nervous system. Nat Rev Neurosci 2003; 4: 121–30.

3 Holgate ST, Canonica GW, Simons FE, Taglialatela M, Tharp M, Timmerman H, Yanai K. Consensus Group on New-Generation Antihistamines (CONGA): present status and recommendations. Clin Exp Allergy 2003; 33: 1305–24.

4 Casale TB, Blaiss MS, Gelfand E, Gilmore T, Harvey PD, Hindmarch I, Simons FE, Spangler DL, Szefler SJ, Terndrup TE, Waldman SA, Weiler J, Wong DF. First do no harm: managing antihistamine impairment in patients with allergic rhinitis. J Allergy Clin Immunol 2003; 111: S835–42.

5 Brown RE, Stevens DR, Haas HL. The physiology of brain histamine. Prog Neurobiol 2001; 63: 637–72.

6 Yanai K, Ryu JH, Watanabe T, Iwata R, Ido T, Sawai Y, Ito K, Itoh M. Histamine H1 receptor occupancy in human brains after single oral doses of histamine H1 antagonists measured by positron emission tomography. Br J Pharmacol 1995; 116: 1649–55.

7 Okamura N, Yanai K, Higuchi M, Sakai J, Iwata R, Ido T, Sasaki H, Watanabe T, Itoh M. Functional neuroimaging of cognition impaired by a classical antihistamine, d-chlorpheniramine. Br J Pharmacol 2000; 129: 115–23.

8 Tagawa M, Kano M, Okamura N, Higuchi M, Matsuda M, Mizuki Y, Arai H, Iwata R, Fujii T, Komemushi S, Ido T, Itoh M,

Sasaki H, Watanabe T, Yanai K. Neuroimaging of histamine H1-receptor occupancy in human brain by positron emission tomography (PET): a comparative study of ebastine, a second-generation antihistamine, and (+)-chlorpheniramine, a classical antihistamine. Br J Clin Pharmacol 2001; 52: 501–9.

9 Tashiro M, Sakurada Y, Iwabuchi K, Mochizuki H, Kato M, Aoki M, Funaki Y, Itoh M, Iwata R, Wong DF, Yanai K. Central effects of fexofenadine and cetirizine: measurement of psychomotor performance, subjective sleepiness, and brain histamine H1-receptor occupancy using 11C-doxepin positron emission tomography. J Clin Pharmacol 2004; 44: 890–900.

10 Tashiro M, Mochizuki H, Sakurada Y, Ishii K, Oda K, Kimura Y, Sasaki T, Ishiwata K, Yanai K. Brain histamine H receptor occupancy of orally administered antihistamines measured by positron emission tomography with (11)C-doxepin in a placebo-controlled crossover study design in healthy subjects: a comparison of olopatadine and ketotifen. Br J Clin Pharmacol 2006; 61: 16–26.

11 Ishibashi Y, Kawashima M, Harada S, Suzuki Y. [Phase I study of antiallergic agent, TAU-284 (betotastine besilate): study of inhibitory effect on intradermal reaction of histamine]. J Clin Therap Med 1997; 13: 53–63.

12 Yokota H, Mizuuchi H, Maki T, Banno K, Sato T. [Phase I study of TAU-284: single oral administration in healthy male volunteers]. J Clin Therap Med 1997; 13: 3–19.

13 Kawashima M, Harada S, Nakajima M. [Phase III study of TAU-284 (betotastine besilate) on chronic urticaria: a multicenter double blind comparative study with placebo]. J Clin Therap Med 2002; 18: 13–31.

14 Murata T, Matsumoto Y, Suzuki T, Naito K, Takata I, Tsuzurahara K. [Effect of betotastine besilate (TAU-284), a novel anti-allergic agent, on experimental allergic rhinitis]. Arerugi 1997; 46: 576–84.

15 Yato N, Murata T, Saito N, Sakai A, Kikuchi M, Tsuzurahara K, Narita H. [Anti-allergic activity of betotastine besilate (TAU-284), a new anti-allergic drug]. Nippon Yakurigaku Zasshi 1997; 110: 19–29.

16 Ueno M, Inagaki N, Nagai H, Koda A. Antiallergic action of betotastine besilate (TAU-284) in animal models: a comparison with ketotifen. Pharmacology 1998; 57: 206–14.

17 Nakahara T, Urabe K, Moroi Y, Morita K, Furue M. Bepotastine besilate rapidly inhibits mite-antigen induced immediate reactions in atopic dermatitis. J Dermatol Sci 2003; 32: 237–8.

18 Takahashi H, Ishida-Yamamoto A, Iizuka H. Effects of bepotastine, cetirizine, fexofenadine, and olopatadine on histamine-induced wheal-and flare-response, sedation, and psychomotor performance. Clin Exp Dermatol 2004; 29: 526–32.

19 Kato M, Nishida A, Aga Y, Kita J, Kudo Y, Narita H, Endo T. Pharmacokinetic and pharmacodynamic evaluation of central effect of the novel antiallergic agent betotastine besilate. Arzneimittelforschung 1997; 47: 1116–24.

20 Kay GG, Harris AG. Loratadine: a non-sedating antihistamine. Review of its effects on cognition, psychomotor performance, mood and sedation. Clin Exp Allergy 1999; 29 (Suppl. 3): 147–50.

21 Tagawa M, Kano M, Okamura N, Higuchi M, Matsuda M, Mizuki Y, Arai H, Fujii T, Komemushi S, Itoh M, Sasaki H, Watanabe T, Yanai K. Differential cognitive effects of ebastine and (+)-chlorpheniramine in healthy subjects: correlation between cognitive impairment and plasma drug concentration. Br J Clin Pharmacol 2002; 53: 296–304.

22 Hindmarch I, Shamsi Z, Kimber S. An evaluation of the effects of high-dose fexofenadine on the central nervous system: a double-blind, placebo-controlled study in healthy volunteers. Clin Exp Allergy 2002; 32: 133–9.

23 Tashiro M, Horikawa E, Mochizuki H, Sakurada Y, Kato M, Inokuchi T, Ridout F, Hindmarch I, Yanai K. Effects of fexofenadine and hydroxyzine on brake reaction time during car-driving with cellular phone use. Hum Psychopharmacol 2005; 20: 501–9.

24 Kumar S, Rurak DW, Riggs KW. Simultaneous determination of diphenhydramine, its N-oxide metabolite and their deuterium-labeled analogues in ovine plasma and urine using liquid chromatography/electrospray tandem mass spectrometry. J Mass Spectrom 1998; 33: 1171–81.

25 Kanba S, Richelson E. Histamine H1 receptors in human brain labelled with [3H]doxepin. Brain Res 1984; 304: 1–7.

26 Inoue I, Yanai K, Kitamura D, Taniuchi I, Kobayashi T, Niimura K, Watanabe T, Watanabe T. Impaired locomotor activity and exploratory behavior in mice lacking histamine H1 receptors. Proc Natl Acad Sci USA 1996; 93: 13316–20.

27 Iwata R, Pascali C, Bogni A, Miyake Y, Yanai K, Ido T. A simple loop method for the automated preparation of (11C) raclopride from (11C) methyl triflate. Appl Radiat Isot 2001; 55: 17–22.

28 Nakamura T, Hayashi Y, Watabe H, Matsumoto M, Horikawa T, Fujiwara T, Ito M, Yanai K. Estimation of organ cumulated activities and absorbed doses on intakes of several 11C labelled radiopharmaceuticals from external measurement with thermoluminescent dosimeters. Phys Med Biol 1998; 43: 389–405.

29 Fujiwara T, Watanuki S, Yamamoto S, Miyake M, Seo S, Itoh M, Ishii K, Orihara H, Fukuda H, Satoh T, Kitamura K, Tanaka K, Takahashi S. Performance evaluation of a large axial field-of-view PET scanner SET-2400w. Ann Nucl Med 1997; 11: 307–13.

30 Bergstrom M, Eriksson L, Bohm C, Blomqvist G, Litton J. Correction for scattered radiation in a ring detector positron camera by integral transformation of the projections. J Comput Assist Tomogr 1983; 7: 42–50.

31 Inoue T, Oriuchi N, Kunio M, Tomiyoshi K, Tomaru Y, Aoyagi K, Amano S, Suzuki H, Aoki J, Sato T, Endo K. Accuracy of standardized uptake value measured by simultaneous emission and transmission scanning in PET oncology. Nucl Med Commun 1999; 20: 849–57.

32 Mochizuki H, Kimura Y, Ishii K, Oda K, Sasaki T, Tashiro M, Yanai K, Ishiwata K. Simplified PET measurement for evaluating histamine H1 receptors in human brains using [11C]doxepin. Nucl Med Biol 2004; 31: 1005–11.

33 Friston KJ, Holmes AP, Worsley KJ, Poline JP, Frith CD, Frackowiak RSJ. Statistical parametric maps in functional imaging: a general linear approach. Hum Brain Mapp 1995; 2: 189–210.

34 Martinez D, Hwang D, Mawlawi O, Slifstein M, Kent J, Simpson N, Parsey RV, Hashimoto T, Huang Y, Shinn A, Van Heertum R, Abi-Dargham A, Caltabiano S, Malizia A, Cowley H, Mann JJ, Laruelle M. Differential occupancy of somatodendritic and postsynaptic 5HT (1A) receptors by pindolol: a dose-occupancy study with [11C]WAY 100635 and positron emission tomography in humans. Neuropsychopharmacology 2001; 24: 209–29.

35 Rabiner EA, Wilkins MR, Turkheimer F, Gunn RN, de Haes JU, de Vries M, Grasby PM. 5-Hydroxytryptamine1A receptor occupancy by novel full antagonist 2-[4-[4-(7-chloro-2,3-dihydro-1,4-benzdioxyn-5-yl)-1-piperazinyl]butyl]-1,2-benzisothiazol-3-(2H)-one-1,1-dioxide: a[11C][O-methyl-3H]-N-(2-(4-(2-methoxyphenyl)-1-piperazinyl) ethyl) -N-(2-py ridinyl) cyclohexanecarboxamide trihydrochloride (WAY-100635) positron emission tomography study in humans. J Pharmacol Exp Ther 2002; 301: 1144–50.

36 Talairach J, Tournoux P. Co-planar Stereotaxic Atlas of the Human Brain. Stuttgart: Georg Thieme Verlag, 1988.

37 van Rij CM, Huitema AD, Swart EL, Greuter HN, Lammertsma AA, van Loenen AC, Franssen EJ. Population plasma pharmacokinetics of 11C-flumazenil at tracer concentrations. Br J Clin Pharmacol 2005; 60: 477–85.

38 Martinez D, Broft A, Laruelle M. Imaging neurochemical endophenotypes: promises and pitfalls. Pharmacogenomics 2001; 2: 223–37.

39 Yanai K, Okamura N, Tagawa M, Itoh M, Watanabe T. New findings in pharmacological effects induced by antihistamines: from PET studies to knock-out mice. Clin Exp Allergy 1999; 29 (Suppl. 3): 29–36; discussion 37–8.

40 Yanai K, Ryu JH, Watanabe T, Iwata R, Ido T, Asakura M, Matsumura R, Itoh M. Positron emission tomographic study of central histamine H1-receptor occupancy in human subjects treated with epinastine, a second-generation antihistamine. Methods Find Exp Clin Pharmacol 1995; 17 (Suppl. C): 64–9.

41 Hindmarch I, Shamsi Z, Stanley N, Fairweather DB. A double-blind, placebo-controlled investigation of the effects of fexofenadine, loratadine and promethazine on cognitive and psychomotor function. Br J Clin Pharmacol 1999; 48: 200–6.

42 Dogan AS, Catafau AM, Zhou Y, Yanai K, Ravert H, Brasic J, Hilton J, Dannals B, Offord S, Wong DF. *In vivo* cerebral histamine receptor occupancy of three antihistamine drugs: an 11C-doxepin PET study. J Nucl Med 2001; 42: 143P–144P.

43 Ohashi R, Kamikozawa Y, Sugiura M, Fukuda H, Yabuuchi H, Tamai I. Effect of P-glycoprotein on intestinal absorption and brain penetration of antiallergic agent bepotastine besilate. Drug Metab Dispos 2006; 34: 793–9.

44 Cvetkovic M, Leake B, Fromm MF, Wilkinson GR, Kim RB. OATP and P-glycoprotein transporters mediate the cellular uptake and excretion of fexofenadine. Drug Metab Dispos 1999; 27: 866–71.

45 Nozawa T, Imai K, Nezu J, Tsuji A, Tamai I. Functional characterization of pH-sensitive organic anion transporting polypeptide OATP-B in human. J Pharmacol Exp Ther 2004; 308: 438–45.

Methods 45 (2008) 300–306

Contents lists available at ScienceDirect

Methods

journal homepage: www.elsevier.com/locate/ymeth

Application of positron emission tomography to neuroimaging in sports sciences

Manabu Tashiro [a,*], Masatoshi Itoh [a], Toshihiko Fujimoto [b], Md. Mehedi Masud [a,b], Shoichi Watanuki [a], Kazuhiko Yanai [a,c]

[a] Division of Cyclotron Nuclear Medicine, Cyclotron and Radioisotope Center, Tohoku University, Aoba 6-3, Aramaki, Aoba-ku, Sendai-shi, Miyagi-ken, Japan
[b] Center for the Advancement of Higher Education, Tohoku University, Sendai, Japan
[c] Department of Pharmacology, Graduate School of Medicine, Tohoku University, Sendai, Japan

ARTICLE INFO

Article history:
Accepted 5 May 2008
Available online 6 June 2008

Keywords:
Cerebral metabolic rate of glucose (CMRglc)
Cerebral blood flow (CBF)
[^{18}F]Fluorodeoxyglucose ([^{18}F]FDG)
Positron emission tomography (PET)
Radio-labelled water ([^{15}O]H_2O)
Exercise
Sports sciences
Neuroimaging

ABSTRACT

To investigate exercise-induced regional metabolic and perfusion changes in the human brain, various methods are available, such as positron emission tomography (PET), functional magnetic resonance imaging (fMRI), near-infrared spectroscopy (NIRS) and electroencephalography (EEG). In this paper, details of methods of metabolic measurement using PET, [^{18}F]fluorodeoxyglucose ([^{18}F]FDG) and [^{15}O]radio-labelled water ([^{15}O]H_2O) will be explained.

Functional neuroimaging in the field of neuroscience was started in the 1970s using an autoradiography technique on experimental animals. The first human functional neuroimaging exercise study was conducted in 1987 using a rough measurement system known as ^{133}Xe inhalation. Although the data was useful, more detailed and exact functional neuroimaging, especially with respect to spatial resolution, was achieved by positron emission tomography. Early studies measured the cerebral blood flow changes during exercise. Recently, PET was made more applicable to exercise physiology and psychology by the use of the tracer [^{18}F]FDG. This technique allowed subjects to be scanned after an exercise task is completed but still obtain data from the exercise itself, which is similar to autoradiography studies.

In this report, methodological information is provided with respect to the recommended protocol design, the selection of the scanning mode, how to evaluate the cerebral glucose metabolism and how to interpret the regional brain activity using voxel-by-voxel analysis and regions of interest techniques (ROI). Considering the important role of exercise in health promotion, further efforts in this line of research should be encouraged in order to better understand health behavior. Although the number of research papers is still limited, recent work has indicated that the [^{18}F]FDG-PET technique is a useful tool to understand brain activity during exercise.

1. Methodologies for functional neuroimaging on exercise

Physical exercise is executed through a sophisticated neural control system in the brain. Neural processing in the human brain plays crucial roles not only in the generation of motor outputs but also in the perception and integration of various sensory inputs. There are various methods for functional neuroimaging, such as positron emission tomography (PET) and single photon emission computed tomography, as well as other imaging methods, such as functional magnetic resonance imaging (MRI), near-infrared spectroscopy (NIRS) and electroencephalography (EEG) (Fig. 1).

We have been using PET, over the last years for measuring the regional metabolism of the brain [1,2] and skeletal muscles during exercise [3,4]. PET has been a useful tool for measuring cerebral metabolic changes induced by exercise tasks. This is especially true for PET procedures that utilize the radio-labelled glucose analogue ([^{18}F]fluorodeoxyglucose: [^{18}F]FDG). This [^{18}F]nuclide has a half-life of approximately 110 min, and such [^{18}F]labelled tracers are suitable for long observation in the range of 30–60 min. Activated regional brain activity is usually accompanied by increased demand for glucose and oxygen, which is immediately followed by dilation of brain capillaries due to increased regional cerebral perfusion (Fig. 1). Thus, cerebral perfusion can be measured using radio-labelled water ([^{15}O]H_2O), that circulates throughout the subject's body intermixed with systemic circulation so that the regions with increased perfusion show increased signals. Although PET together with [^{15}O]H_2O has been used to study brain activation during exercise, it is cumbersome and has some restrictions, that is, subjects have to exercise in the supine position during PET examinations [5–8]. This is unnatural and allows for only limited movement. Partly because of the very short half-life of [^{15}O]nuclide (approximately 2 min), the PET method using [^{15}O]H_2O is not suitable for long observation. In addition, the PET technique has the

* Corresponding author. Fax: +81 22 795 7797.
E-mail address: mtashiro@m.tains.tohoku.ac.jp (M. Tashiro).

1046-2023/$ - see front matter © 2008 Elsevier Inc. All rights reserved.
doi:10.1016/j.ymeth.2008.05.001

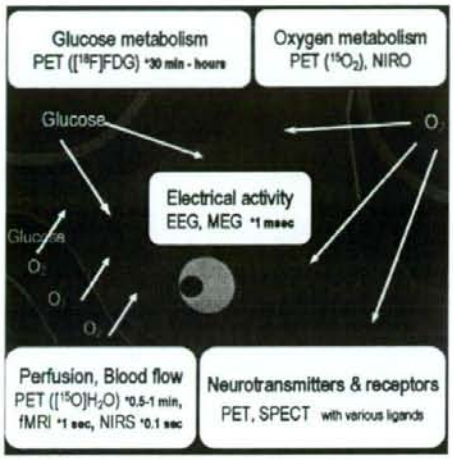

Fig. 1. Methodologies for neuroimaging and biological information obtainable from the living human brain. The most important energy resource of the human brain is glucose. Glucose metabolism can be measured using positron emission tomography (PET) with [^{18}F]fluorodeoxyglucose ([^{18}F]FDG). Temporal resolution of this method is approximately 30 min to a few hours. Oxygen is necessary for the operation of TCSA cycle to synthesize ATP molecules from glucose. Oxygen metabolism can be measured using PET with [^{15}O]O_2 and near-infrared oxymeter (NIRO). Glucose and oxygen molecules necessary for glucose metabolism are supplied by the blood flow. Brain regions with increased activity are accompanied by increased regional cerebral blood flow due to capillary dilation. At present, regional cerebral blood flow changes can be measured using various methods such as PET with [^{15}O]H_2O, functional MRI (fMRI) and near-infrared spectroscopy (NIRS). Temporal resolution of each method is 0.5–1 min, 1 s and 0.1 s, respectively. Interaction of neurotransmitters and receptors can also be measured using PET with various [^{11}C] and [^{18}F] labelled ligands.

hazard of radiation exposure and the number of repeated measurement is therefore limited, which is not the case for MRI, NIRS and EEG.

More recently, methods free from radiation exposure have been introduced. MRI (i.e., fMRI), with higher spatial and temporal resolution, has been applied to the measurement of regional perfusion alterations in the brain, though this method is more vulnerable to motion artifact compared to PET. In addition, another technique, NIRS, has also been recently introduced for measuring regional changes in brain activity, though its spatial resolution is limited and it does not measure well subcortical activation. PET measurement of regional activation using [^{15}O]H_2O is currently limited and it has been more commonly used for measuring regional brain glucose consumption and for evaluating neurotransmission function [9–12]. In this paper, the applications of PET neuroimaging in sports sciences are discussed in more detail (Fig. 1).

As mentioned above, PET has been used for measuring regional brain activity during or following exercise tasks using various radioactive pharmaceuticals such as [^{18}F]FDG and [^{15}O]H_2O. In the human brain, neurotransmitters can manifest their effects even in very small amounts. However, it is not easy to visualize their actions in the living human brain externally without using a highly sensitive technique such as PET. Although neurotransmission studies during exercise are still few, it is possible to quantify interactions between neurotransmitters and neuroreceptors in the living brain using the time course data of radioactivity in brain tissue [13].

2. A brief history of functional neuroimaging during exercise

Regional cerebral metabolic changes induced by exercise have been examined in animals using autoradiography technique such as [^{14}C]deoxyglucose ([^{14}C]2-DG) [14,15]. These studies provided the first functional indices of brain activity with respect to exercise. [^{14}C]2-DG has been a useful tracer for exercise studies because it does not require the simultaneous scanning of subjects during an exercise task [16]. Using this autoradiography technique, Sharp [17] demonstrated a selective increase in glucose uptake in the cerebellar vermis of swimming rats. On the other hand, an autoradiographic study in free-running rats showed no selective activity in the cerebellar vermis but moderately increased glucose uptake for the entire cerebellum [18].

Later, human studies were also conducted. As far as we know, the first study on human brain activity during exercise was conducted by Herholz and coworkers in 1987 [19]. In this study, subjects were examined during a riding task in the half-upright posture (about 45°) using the ^{133}Xe clearance method for studying regional changes in brain activity. They demonstrated that the largest increase in blood flow induced by an ergometer bicycle task was not in the parietal region but in the frontal region. The study had many limitations, such as low spatial resolution (a few centimeters) as well as problems with the study design. Fink and coworkers demonstrated regional activation during and immediately after an ergometer task by PET using [^{15}O]H_2O. The spatial resolution of that study was much better (around 5 mm). They showed activation in the superomedial part of the motor cortex associated with leg and arm motion, which disappeared immediately following the cessation of the motor task, while the lateral part of the motor cortex remained active possibly due to chest wall movement associated with post-exercise hyperventilation [5]. Based on the fact that muscle fibers and motor neurons jointly form "motor units", [^{18}F]FDG uptake in muscles may correlate with activity in their corresponding cerebral regions. Mishina and coworkers applied [^{18}F]FDG-PET to the neuropathological evaluation of patients with olivo-pontine-cerebellar atrophy manifesting gait disturbances who exhibited a decreased response to a walking task in the cerebellar vermis compared with normal subjects [20].

We first applied [^{18}F]FDG-PET to human subjects during a running task in the upright posture [1], and demonstrated augmented energy consumption in the parieto-occipital region during the task compared with the motor area. This was probably due to the higher energy consumption necessary for integrating multimodal sensory information. Our results also showed that frontal activity was lower during running than during resting. In addition, our study demonstrated a trend of relative decrease in whole brain mean activity during exercise compared with the resting condition. In parallel, our group also examined whole-body energy (glucose) redistribution and how exercise affects this distribution. We showed no significant changes in relative glucose metabolism in the brain between exercise and resting conditions [21]. Based on the work by Tashiro and coworkers [1], Kemppainen and coworkers examined absolute glucose consumption in the human brain of healthy volunteers. They found for the first time, using [^{18}F]FDG-PET technique, that the glucose consumption level decreases during strenuous exercise especially in the cingulate gyrus [2].

3. Measurement of cerebral glucose metabolism

The autoradiographic technique using [^{14}C]2-DG has been a useful tracer for exercise studies because it does not require simultaneous scanning of subjects during an exercise task [16]. The metabolic alteration is trapped, which enables the observation of the remaining metabolic "record" or "memory" afterward. With this technique, data acquisition can be performed following exercise tasks although the data "dates back" to the exercise itself. However, the [^{14}C]2-DG is not applicable to human activation studies because its half-life is too long. Mishina and coworkers measured

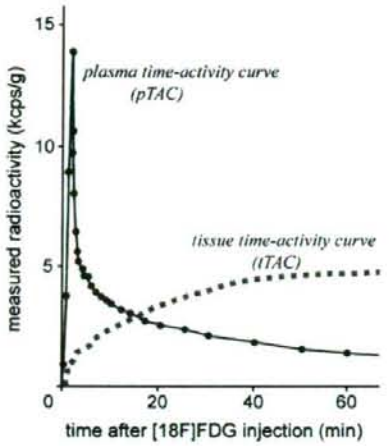

Fig. 2. Time–activity curves in plasma (pTAC: solid line) and tissue (tTAC: dotted line) following [^{18}F]FDG injection. The plasma concentration of [^{18}F]FDG is very high for the first 10 min or so after injection, and then gradually decreases. Therefore, it is recommended that exercise tasks be completed within the first 30 min or so. [^{18}F]FDG accumulation in the tissue (brain) reaches a plateau after 30–40 min following injection. A prolonged exercise task lasting for 60 min after injection does not produce additional accumulation since the plasma concentration of [^{18}F]FDG is already very low; instead, blood with low [^{18}F]FDG concentration might wash out the FDG particularly after 60 min of injection. Abbreviation: kcps, kilo-count per second.

cerebellar glucose uptake before and after walking in patients with neurological disorders using [^{18}F]FDG [20]. Although their main purpose was the clinical evaluation of a specific neurological disorder, this is probably the first study conducted in human subjects to investigate the effect of actual walking on brain activity. Thus, [^{18}F]FDG has proven to be an ideal tracer for exercise physiology studies in humans because of its metabolic trapping property, a property that has already been recognized together with [^{14}C]2-DG, for that purpose. When this tracer is used, the [^{18}F]FDG molecules are taken up by activated regional brain or muscle tissues in proportion to the energy consumption level of these tissues. Then, the [^{18}F]FDG molecules are phosphorylated in a manner similar to a glucose molecule. However, these [^{18}F]FDG molecules escape from further metabolism and are eventually trapped in the tissue, preserving the metabolic pattern for an hour or so [16]. Thus, it is possible to estimate energy consumption in different regions of the brain an hour after the completion of physical activity.

As shown in Fig. 2, the plasma time–activity curve (pTAC) demonstrates that the plasma [^{18}F]FDG concentration is very high for the first 10 min or so after injection, and then gradually decreases. Therefore, it is recommended that some kind of exercise tasks be conducted during the first 30 min or so. A prolonged exercise task up to 60 min after injection would not produce much difference since the plasma [^{18}F]FDG concentration is already very low. Instead, the blood with low [^{18}F]FDG concentration might wash out the [^{18}F]FDG particularly 60 min after injection. With this in mind, [^{18}F]FDG-PET can be an ideal technique for studies on exercise physiology by separating "a task phase" (the first 30 min or so) and "data acquisition phase" (30–60 min after injection). This paradigm allows investigation of a totally free movement task assigned to subjects. NIRS also allows observation of moving subjects; however, the subjects are connected to the data acquisition system by a measurement cap and cables, requiring proximity to the system for any tasks to be performed. Also, it is prone movement artifacts for gross movements. With the [^{18}F]FDG-PET technique, subjects can carry out any tasks, that is, not only running but any movement such as driving of a car or swimming [22]. Thus, although the temporal resolution of the [^{18}F]FDG-PET technique is limited (just 30–60 min), it is exactly this unique property that enables the application of this technique to human movement science.

As for the cellular and molecular mechanism of the [^{18}F]FDG-PET and autoradiography techniques, new studies have added several novel findings. Brain glucose/[^{18}F]FDG was thought to be transported and consumed by neural cells. However, recent studies have demonstrated that glucose/[^{18}F]FDG is transported through the blood–brain barrier (BBB) to be taken up by astrocytes, which express a large number of glucose transporters (GLUT) of GLUT-1 type on their surface membranes. It has been proposed that neurons receive their energy source from these astrocytes in the form of lactate produced by glycolysis and lactate dehydrogenase action [23–25]. Magistretti and Pellerin have established the "astrocyte-neuron lactate shuttle hypothesis" (ANLSH), an operational model for the coupling between synaptic activity and glucose utilization. This model seems to be consistent with the notion that the signals detected during brain activation studies using [^{18}F]FDG-PET may predominantly reflect tracer uptake not into neurons but into astrocytes [23–25]. This theory has provided a cellular and molecular basis for these functional brain imaging techniques; however, it does not question the validity of brain activation techniques using [^{18}F]FDG and [^{14}C]2-DG [23–25].

4. Data acquisition and two- and three-dimensional modes

PET is the method of choice for functional imaging using radiopharmaceuticals that detect annihilation photons with relatively high energy (511 keV) emitted from injected radioisotopes. Recent technical advances have allowed the development of a new three-dimensional (3D) data acquisition mode system with increased sensitivity of up to about 8–10 times that of a conventional two-dimensional (2D) mode system [26]. This significant increase in sensitivity has lead to a substantial reduction in radiological doses and therefore reduction in radiation exposure to subjects. With this innovation, studies on healthy volunteers using PET have become more feasible than before. Thus, we first applied this technique to map changes in whole-body glucose metabolism during running in the upright posture [3], and assessed skeletal muscle activity in normal healthy volunteers [4]. Usually, [^{18}F]FDG of 190–370 MBq (5–10 mCi) is injected to patients for clinical diagnosis using 2D acquisition mode. Since the effective doses in humans using [^{18}F]FDG is estimated as 0.02 mSv/MBq or so (0.8 mSv/mCi or so) [27], the radiation exposure to the patients is estimated to be 3.8–7.4 mSv. Using the 3D acquisition mode, 40–80 MBq (1–2 mCi) would be enough for the exercise study however. Thus the radiation exposure to the subjects is far below (0.8–1.6 mSv) the annual accumulated environmental radiation exposure (2.4 mSv). Thus, for safety reasons in terms of radiation, it is recommended to use the 3D acquisition mode for exercise study because it allows for less radiation exposure to otherwise healthy subjects. In addition, depending on the study protocol, a practical way to minimize radiation exposure would be to avoid scanning the same subject more than twice.

5. Protocols for measuring cerebral glucose metabolism during exercise

At many institutes, [^{18}F]FDG is presently synthesized based on the procedure introduced by Hamacher and colleagues [28]. In studies using [^{18}F]FDG, it is expected that all subjects refrain from eating and drinking for at least for 3–4 h before starting the examinations ([^{18}F]FDG injection). If possible, fasting for 5 h would be

ideal because the influx of [^{18}F]FDG molecules into the brain tissue is affected by plasma glucose level, and an increased level of plasma glucose lowers [^{18}F]FDG uptake into the brain because of competition. Thus, plasma glucose concentration should be measured in all subjects just prior to [^{18}F]FDG injection to determine if the glucose level is within the appropriate range. Moreover, subjects should not perform any exercise one day before the examinations. In a previous study by Kemppainen and coworkers, subjects fasted for at least 12 h before the study and any kind of strenuous physical activity was prohibited for at least one day before PET examination [2]. Usually, PET scanning is initiated 40 min after [^{18}F]FDG injection since [^{18}F]FDG uptake in brain tissue reaches the plateau level at around 40–50 min post-injection. Also, it is recommended to recruit subjects who are all right-handed or left-handed because some studies have suggested effects of lateralization of specific sensori-motor functions [29,30]. Our previous study suggested the presence of lateralization in muscular glucose metabolism used during upright running [1].

Usually, subjects are instructed to run for a total of 30–40 min after [^{18}F]FDG injection, with 10–15 min of exercise before injection. The amount of injected [^{18}F]FDG is approximately 40–80 MBq (1–2 mCi per subject) if a 3D data acquisition system is used. If a 2D system is used, 200 MBq [^{18}F]FDG (approximately 5 mCi) is needed for data acquisition to compensate for the lower sensitivity of the detector system. For [^{18}F]FDG injection, a catheter is usually inserted into an antecubital forearm vein. For quantification of absolute glucose consumption rate, another catheter should be, in principle, inserted in the artery of the opposite arm for serial sampling of arterial blood. Some investigators also use arterialized venous blood data using the opposite antecubital vein. In this case, the forearm should be warmed so that as many arterio-venous shunts are opened as possible. In order to observe "relative" cerebral glucose metabolic changes, however, investigators do not have to carry out serial blood sampling.

Following an exercise task, PET scanning is initiated. There are two kinds of scanning modes, namely, "emission" and "transmission" scans. In emission scanning, annihilation photons (gamma rays of 511 keV) emitted from the injected radiopharmaceuticals in the body of subjects are detected by the PET detector system. In transmission scanning, external radiation sources such as ^{68}Ge/^{68}Ga emitting 511 keV gamma rays are detected by PET detectors to map the tissue attenuation throughout the brain. These transmission data are used for correcting the emission data affected by tissue attenuation [26]. As indicated in Fig. 4, the deeper the location of the brain structure, the more the counts are attenuated due to absorption and diffraction in the brain and surrounding tissues. For the data analysis, images corrected for tissue attenuation should be used.

6. Quantification of cerebral metabolic rate of glucose

Quantification of regional cerebral metabolic rate of glucose (rCMRglc) is done based on the method developed by Sokoloff and coworkers, who used the equation below based on a compartment model consisting of three compartments for "[^{18}F]FDG in plasma", "unmetabolized [^{18}F]FDG in the brain" and "metabolized [^{18}F]FDG in the brain", as shown in Fig. 3 [31,32]:

$$\mathrm{CMRglc} = \frac{C_p}{LC}\left[\frac{k_1^* k_3^*}{k_2^* + k_3^*}\right]\left[\frac{C_i^*(T) - C_e^*(T)}{C_m^*(T)}\right]$$

where C_p denotes native glucose concentration in plasma, LC denotes the lumped constant for [^{18}F]FDG, k_1^* to k_3^* denote the first order kinetic rate constants for [^{18}F]FDG, $[C_i^*(T) - C_e^*(T)]/C_m^*(T)$ is the factor that corrects the ratio between observed and the population-average metabolic rates [31,32]. For the calculation of

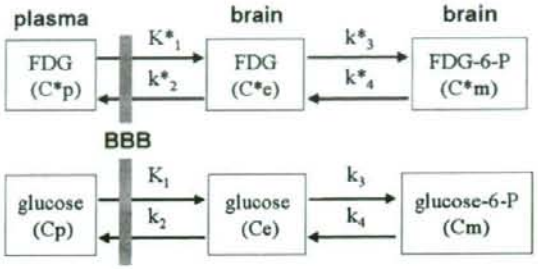

Fig. 3. Schematic diagram demonstrating the kinetic model for quantification of regional cerebral metabolic rate of glucose (rCMRglc). This compartment model consists of three compartments for "FDG in plasma", "unmetabolized FDG in the brain" and "metabolized FDG in the brain". C_p, C_e and C_m denote concentrations of native glucose in plasma and the brain tissue, and metabolized glucose (glucose 6-phosphate, glucose-6-P), respectively. C_p^*, C_e^* and C_m^* denote concentrations of FDG in plasma and the brain tissue, and metabolized FDG (FDG 6-phosphate, FDG-6-P), respectively. k_1 to k_4 denote the first-order kinetic rate constants for glucose. k_1^* to k_4^* denote the first-order kinetic rate constants for FDG. Abbreviation: BBB, blood–brain barrier.

rCMRglc, LC of 0.52, reported by Reivich and coworkers, is often used [33]. Recently, Wakita and coworkers established a simplified quantification technique using 1-point blood sampling data using arterial (12 min after injection) and venous (40 min after injection) blood [34]. In addition to the method for quantifying rCMRglc based on the full kinetic model [35,36], simplified graphical analytic methods are also available. The latter is used in PET scans performed after exercise (lacking the first part of the time–activity curve), as reported in the study by Kemppainen and coworkers [2]. In the first quantification study conducted by Kemppainen and coworkers, plasma radioactivity tended to be low 25 min after tracer injection and exercise. This suggests that the period between the end of exercise and the start of the scan had a minor effect on cerebral tissue tracer counts [2], which indicated that the measured k_i reflects the existing condition during exercise.

In addition to the determination of rCMRglc, rough estimation of [^{18}F]FDG distribution is also sometimes used to identify changes in global mean glucose metabolism. Tashiro and coworkers previously calculated the modified standardized uptake ratio (SUR) (also known as standardized uptake value, SUV), which represents the ratio of the global mean cerebral glucose uptake to the whole body [^{18}F]FDG uptake, using the following equation:

$$\mathrm{SURm} = \frac{\text{global mean cerebral [}^{18}\text{F]FDG uptake per volume (cps/pixel)}}{\text{mean whole body [}^{18}\text{F]FDG uptake per volume (cps/pixel)}}$$

A basic equation is introduced by Kubota and coworkers as follows [37]:

$$\mathrm{SUR} = \frac{[^{18}\text{F]FDG uptake per volume (cps/pixel)} * \text{body size of subjects (kg)}}{\text{injected dose(MBq)} * \text{calibration factor(cps/MBq)}}$$

7. Voxel-by-voxel analysis using statistical parametric mapping

Voxel-by-voxel analysis is the standard tool in detecting changes in activity levels in certain brain regions. The most popular contrast in exercise studies has been to contrast "resting" with "active exercise". In addition, voxel-by-voxel analysis as been useful in detecting brain regions correlating with specific cofounding factors such as age, exercise intensity, as well as measures of blood chemistry and autonomic nervous function. As demonstrated in previous exercise studies [1,2], the most popular software tool for this analysis has been the "Statistical Parametric Mapping (SPM)" software package.

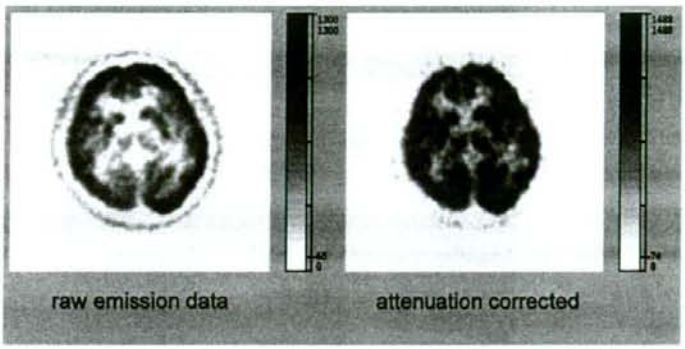

Fig. 4. Brain images with and without attenuation correction. Rawemission data (LEFT) have low signals in the middle part of the brain due to increased tissue attenuation. This tissue attenuation can be corrected using transmission data. The corrected image is shown in the right hand of this figure.

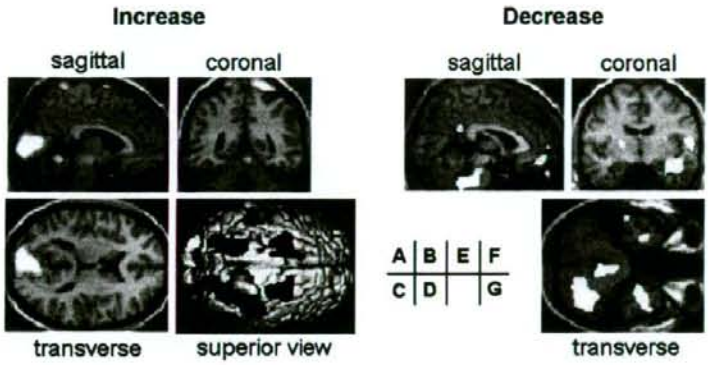

Fig. 5. Voxel-by-voxel analysis can visualize both increased and decreased regional brain activities associated with exercise task. Areas of significantly increased (LEFT) and decreased (RIGHT) glucose metabolisms during running, where the areas with statistically-significant changes appear in red to yellow. Sagittal section image (A) showing high glucose uptake in the posterior parietal, occipital visual and premotor cortices, and cerebellar vermis. Coronal section image (B) showing high uptake in the posterior parietal cortex and cerebellar vermis. Transverse sectional image (C) showing high uptake in the occipital visual cortex. Surface rendering image providing superior (vertex) view which demonstrates high uptake in the premotor, temporo-parieto-occipital association and visual cortices (D). Sagittal section image (E) on the right showing low uptake in the basal prefrontal cortex. Coronal section image (F) showing low uptake in the temporal lobe including the basal ganglia. Transverse section image (G) showing low uptake in the cerebellar hemisphere and inferoanterior temporal regions. Modified from the Ref. [1] by courtesy of Minerva Medica.

Briefly, the brain parametric images of each individual are realigned across different conditions using parameters estimated from summed images. For statistical analysis, all brain images were anatomically normalized by mathematical calculation including linear and non-linear transformations to minimize inter-subject anatomical variation using the SPM software package [38]. This normalization procedure is executed based on MRI T1 image of each subject's own or a ligand-specific template for [^{18}F]FDG that is available from the SPM site. In the work by Kemppainen et al. [2], the brain images were then smoothed using a 12- to 16-mm isotropic Gaussian kernel to increase the signal-to-noise ratio, depending on the spatial resolution of the PET scanner. For statistical analysis, all pixel values were normalized to an arbitrary global mean value of 50 mg/100 ml/min by ANCOVA to exclude the effects of inter-subject variability in global cerebral glucose metabolism. The paired *t*-test was applied to each voxel; only voxel clusters were maintained with voxels corresponding to $p < 0.001$ in a single test and a cluster size of 8 voxel minimum in two ways (runners-controls and controls-runners) [39]. The statistical significance of a regional metabolic change was given in Z scores. Empirically in SPM analysis, a Z score higher than 3.0 (approximately corresponding to $p < 0.001$) is roughly considered as statistically significant. The location of each statistical peak was identified based on a co-planar stereotaxic atlas of the human brain [40]. Recently, this localization procedure is often carried out using the MNI Space utility, which first converts the MNI coordinates given by SPM to Talairach coordinates using non-linear transformation and then identifies each voxel by the anatomical labels presented in the Talairach Daemon database [41]. Statistically significant areas were superimposed on the standard MRI brain template images (Fig. 5). The adjusted regional metabolic rate ratio at each statistical peak is available by defining regions of interest (ROIs) based on the normalized brain images as demonstrated by the plotted data in Fig. 6 [39]. In principle, the SPM analysis is conducted as an explorative analysis covering the whole brain, that is, without any *a priori* hypothesis or spatial constrictions concerning the location of potential effects. If carried out with a certain *a priori* hypothesis or spatial constrictions concerning the location of potential effects, statistical thresholds can be lowered. In addition, in case the quantitative brain images of glucose metabolic rate (GMR) values are used, SPM analyses should be performed without global normalization function.